# Dielectric Slab-Loaded Resonant Cavity for Applications Requiring Enhanced Field Uniformity

J. T. Bernhard and W. T. Joines

*Abstract*—**This paper introduces and analyzes a rectangular resonant structure that provides an alternative to the multimode resonant cavity in applications requiring enhanced field uniformity. The resonant cavity contains four dielectric loading slabs placed along the cavity walls. Its first resonant mode is related to the uniform field distribution supported in a rectangular TEM waveguide. The electromagnetic fields within the cavity are described using a closed-form approach, with approximations taken to account for the presence of two of the loading slabs. Application of the boundary conditions leads to an eigenvalue formulation, which is used to determine resonant frequencies and electromagnetic field distributions within the cavity. Measurements of both resonant frequencies and electric field magnitudes confirm the analysis. This work provides the basis for future analyses and implementation of slab-loaded cavities in both scientific and industrial settings.**

## I. Introduction

In recent years, interest in using microwave signals for applications in many nontraditional settings and disciplines has grown dramatically. Some of these applications include using microwave power for heat treating, polymer and ceramic curing, and plasma processing [1], [2], as well as to accelerate and influence the course of chemical reactions and to investigate the effects of microwaves on biological tissues [3], [4]. These applications require electromagnetic exposure chambers with relatively uniform power distributions. Uniform power distributions within the chambers help to prevent "hot" or "cold" spots which may cause unnecessary destruction or waste of sample material.

Several researchers [1], [2] have concentrated their efforts toward the design and analysis of multimode resonant cavities to achieve more uniform exposure of samples to microwave fields. These multimode cavities possess fairly uniform power distributions in their central regions. However, a sample placed with its edges near the conducting walls of a cavity experiences steep field gradients, resulting in large discrepancies in exposure across the entire sample. This effectively reduces the usable volume of the exposure chamber, wasting both space and energy. Additionally, the use of large bandwidth swept frequency generators makes the apparatus expensive and inefficient, since power at some frequencies will be reflected back to the source.

This paper introduces and analyzes a rectangular resonant structure which provides an alternative to the multimode resonant cavity in applications that require enhanced field uniformity. The resonant cavity contains four dielectric loading slabs parallel and adjacent to the side walls of the cavity. Its first resonant mode is related to the uniform field distribution supported in a rectangular TEM waveguide. The electromagnetic fields within the cavity are described using a closed-form approach, with approximations taken to account for the presence of two of the loading slabs. Application of the boundary conditions leads to an eigenvalue formulation, which is used to determine resonant frequencies and electromagnetic field distributions within the cavity. Measurements of both resonant frequencies and electric field magnitudes confirm the analysis. This work provides the basis for future analyses and implementation of slab-loaded cavities in both scientific and industrial settings.

Manuscript received November 10, 1994; revised November 27, 1995. This work was supported in part by the National Cancer Institute, DHHS, PHS Grant 2 po1 CA42745-08.

J. T. Bernhard was with the Department of Electrical Engineering, Duke University, Durham, NC 27708-0291. She is now with the Department of Electrical and Computer Engineering, University of New Hampshire, Durham, NH 03824 USA.

W. T. Joines is with the Department of Electrical Engineering, Duke University, Durham, NC 27708-0291 USA.

Publisher Item Identifier S 0018-9480(96)01549-9.

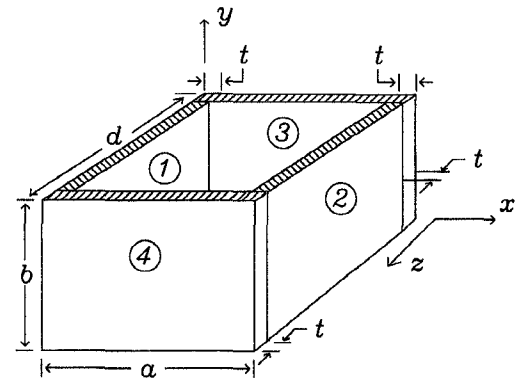


Fig. 1. Inside configuration of the slab-loaded resonant cavity. All dielectric loading slabs have thickness $t$ and height $b$. The rectangular cavity has dimensions of width $a$, height $b$, and length $d$. Dielectric slabs 1 and 2 are oriented along the $\hat{x}$ direction. Dielectric slabs 3 and 4 are oriented along the $\hat{z}$ direction.

## II. Structure

The cavity's structure consists of a rectangular cavity lined on four of the six conducting walls with dielectric loading slabs, as shown in Fig. 1. The cavity has inner dimensions of width $a$, height $b$, and length $d$. The dielectric slabs each have thickness $t$, height $b$, and relative permittivity $\epsilon_1$. Two slabs with length $d - 2t$ (designated as 1 and 2 in Fig. 1) are oriented parallel to the $\hat{z}$ axis, and the remaining two with length $a$ (designated as 3 and 4 in Fig. 1) are oriented parallel to the $\hat{x}$ axis. In this analysis, the inner volume is assumed to be filled with air ($\epsilon_2 \approx 1$).

## III. Theory

Empty rectangular cavities have resonant modes based on TE and TM modes of empty rectangular waveguides. On the other hand, the slab-loaded cavity described in the previous section supports modes based on the longitudinal-section electric (LSE) and longitudinal-section magnetic (LSM) modes of waveguides loaded with two dielectric slabs. The LSE modes have a magnetic field component normal to the dielectric interfaces. The LSM modes have an electric field component normal to the dielectric interfaces [5].

The LSE and LSM modes of a rectangular waveguide loaded with dielectric slabs along $\hat{z}$, with lossless propagation in the $\hat{z}$ direction, are derived from the magnetic and electric Hertzian potentials, respectively, $\vec{\Pi}_h = \hat{x}\psi_h(x, y)e^{-jk_z z}$ and $\vec{\Pi}_e = \hat{x}\psi_e(x, y)e^{-jk_z z}$. For the case of a resonant cavity of length $d$ containing just two dielectric slabs along the $\hat{z}$ direction, the exponential $z$ dependence of $\vec{\Pi}_h$ and $\vec{\Pi}_e$ is changed to a sinusoidal form, determined by the geometry of the structure and boundary conditions. Therefore, $\vec{\Pi}_h = \hat{x}\psi_h(x, y, z)$ and $\vec{\Pi}_e = \hat{x}\psi_e(x, y, z)$. For such potentials satisfying the Lorentz condition, the electric and magnetic fields for

the LSE modes and LSM modes, respectively, are [5]

$$\vec{E}_{\mathrm{LSE}} = -j\omega\mu\nabla \times \vec{\Pi}_h \tag{1}$$

$$\vec{H}_{\mathrm{LSE}} = \nabla \times \nabla \times \vec{\Pi}_h \tag{2}$$

$$\vec{H}_{\mathrm{LSM}} = j\omega\epsilon\nabla \times \vec{\Pi}_e \tag{3}$$

$$\vec{E}_{\mathrm{LSM}} = \nabla \times \nabla \times \vec{\Pi}_e. \tag{4}$$

Both of the Hertzian potentials also satisfy the wave equation

$$\nabla^2\vec{\Pi} + k^2\vec{\Pi} = 0 \tag{5}$$

with $k$ equal to the wave number. The solution of (5), obtained through separation of variables, yields a product of sine and cosine functions in all three dimensions, with corresponding phase constants in the three dimensions, $k_x$, $k_y$, and $k_z$. For a cavity containing *two* loading slabs lengthwise along $\hat{z}$, the structure is divided into three sections: one corresponding to each of the dielectric loading slabs and the one representing the central region. Approximate values of the phase constants may be obtained using the transverse resonance method [5]. Application of the boundary conditions at the perfectly conducting walls and at the dielectric interfaces normal to $\hat{x}$ result in an eigenvalue formulation, from which the resonant frequencies and multiplicative field constants are determined [6], [7].

This method cannot be applied directly to the slab-loaded cavity shown in Fig. 1 due to the presence of dielectric interfaces along not one, but two dimensions. A modification to this method, however, provides good approximations to the resonant frequencies and the associated field distributions of the cavity. This modification utilizes the concept of effective length to account for the two slabs oriented along $\hat{x}$ (designated as 3 and 4 in Fig. 1). As an example, assume that these two slabs have thickness $t$ in the $z$ dimension and a relative permittivity $\epsilon_1$. The effective length of the cavity in the $\hat{z}$ direction, $d'$, is calculated as

$$d' = (d - 2t) + 2t\sqrt{\epsilon_1} \tag{6}$$

with $d - 2t$ equal to the length of the portion of the cavity filled with air in the $\hat{z}$ direction and $2t\sqrt{\epsilon_1}$ equal to the effective electrical length in $\hat{z}$ of the two dielectric slabs. This method provides more accurate results for resonant frequencies and field distributions when the longer cavity dimension ($a$ or $d$) is designated as the $\hat{z}$ dimension, and its effective length is calculated using (6). The field distributions for resonant modes are obtained by calculating the $\hat{x}$-directed component assuming two loading slabs along $\hat{z}$, (designated as 1 and 2 in Fig. 1) and the $\hat{z}$-directed components by taking the effective length of the slabs along $\hat{x}$ (designated as 3 and 4 in Fig. 1) into account. More rigorous solutions for the field distributions may be obtained using mode matching techniques, at the expense of more complex computations.

In empty rectangular resonant cavities, the modes are commonly classified by the type of mode (TE or TM) and the integers $m$, $n$, and $p$ which specify the variations of the fields in the three orthogonal directions, e.g., $\mathrm{TE}_{101}$. The designation for the LSE and LSM modes in the slab-loaded cavity may be described in a similar manner, keeping in mind that the $x$ variation index, $m$, cannot be strictly interpreted for any information other than a general indication of the approximate number of half-sine variations within the entire cross section of the cavity in $x$. Also note that in this case, the $z$ index, $p$, must also be interpreted with caution, since it is specified in the context of the length extension, $d'$. Fig. 2 compares the cross-sectional electric field uniformity achieved in the first resonant mode in the dielectric slab-loaded cavity ($\mathrm{LSE}_{101}$) with that attained within empty resonant cavity ($\mathrm{TE}_{101}$) of the same size. Note that a more uniform field distribution is attainable as the cavity's resonant frequency approaches the operational frequency of the related TEM waveguide, which in this case is 915 MHz.

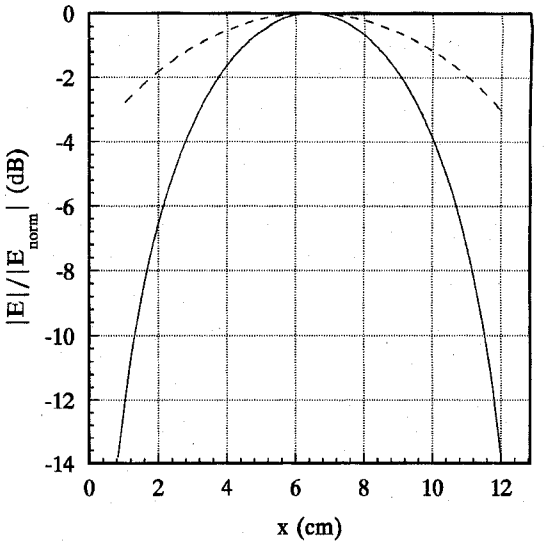


Fig. 2. Normalized variation of electric fields (in dB) over a cross section in $x$ within an empty cavity (—) and a dielectric-slab-loaded cavity (- - -) at their first resonant frequencies.

A microwave cavity operated around any of its resonant frequencies behaves much like a discrete resonant circuit [8]. As with discrete resonant circuits, the quality factor of such a resonant cavity, $Q$, serves as a measure of the sharpness of the system's frequency response. The $Q$ of a resonant system is defined as [9]

$$Q \triangleq \omega_0 \frac{\text{peak energy stored}}{\text{average power lost}} = \omega_0 \frac{U}{W_L}. \tag{7}$$

Estimation of a cavity's $Q$ also has implications for the time required for convergence of numerical models [1].

The $Q$ of the dielectric slab-loaded cavity at any of its resonant frequencies is obtained by calculating the peak stored energy, $U$, and average power lost, $W_L$, at that particular frequency, taking both the conduction loss within the cavity walls and the dielectric loss in the loading slabs into account. Calculation of these quantities requires knowledge of the field distributions of each resonant mode. The derivation of the $Q$ of the slab-loaded cavity of Fig. 1 presents some complications since the resonant electromagnetic fields are approximated through use of the effective length extension, $d'$. Consequently, the propagation constant in the $\hat{z}$ direction, $k_z$, is taken to be $p\pi/d'$. However, the actual propagation constants in the $\hat{z}$ direction are different within the central region and dielectric loading slabs, typically with $k_z$ in the loading slabs being larger than $k_z$ in the central region. Therefore, both the peak stored energy and average power lost in the cavity may be underestimated using this model.

## IV. Measurement

To test the validity of the length extension, $d'$, the field distributions of several resonant modes in a cavity loaded with four dielectric slabs were measured. The cavity was constructed of aluminum and the loading slabs were made of titania obtained from Trans-Tech, Inc., of Adamstown, MD (Dielectric Bulletin no. 65-70), with a thickness, $t$, of 0.841 cm, height of 9.0 cm, and length of 12.0 cm. The relative dielectric constant of these slabs is specified as 96.0 ± 5% with a dielectric loss tangent of less than 0.0001 at 6 GHz. For support, the inner portion of the waveguide was filled with styrofoam, which has a relative dielectric constant approximately equal to unity (typically 1.05–1.10). The inner dimensions of the cavity were as follows:

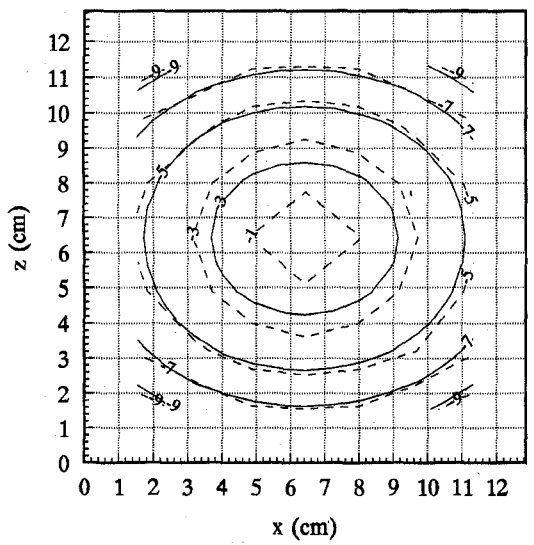


Fig. 3. Relative measured (- - -) and simulated (—) values of $S_{21}$ (in dB), representing values of $\hat{y}$-directed electric field for the $LSE_{101}$ resonant mode of a slab-loaded resonant cavity. The area on the perimeter of the graph that does not contain contour lines (0.0 cm $\leq x \leq$ 0.841 cm, 12.0 cm $\leq x \leq$ 12.841 cm, 0.0 cm $\leq z \leq$ 0.841 cm, 12.0 cm $\leq z \leq$ 12.841 cm) represents the area occupied by the dielectric loading slabs.

TABLE I
SIMULATED AND MEASURED RESONANT FREQUENCIES AND UNLOADED $Q$ FOR THE $LSE_{101}$ MODE OF THE DIELECTRIC SLAB-LOADED CAVITY

| | Simulated | Measured | Percent Error |
|---|---|---|---|
| Resonant Frequency | 866.0 MHz | 873.0 MHz | 0.80 |
| Unloaded $Q$ | 2412.1 | 2028.9 | 18.89 |

$a = d = 12.841$ cm and $b = 9.0$ cm. The effective length of the cavity in $z$, $d'$, is then equal to 27.639 cm according to (6).

The cavity was fed from a centered ($x = z = a/2$, $y = 0$) coaxial probe oriented parallel to the $\hat{y}$ axis of the system to excite the odd order, symmetric LSE modes. Measurements were taken with the HP 8753A Network Analyzer. A measurement of return loss, $S_{11}$, determined the resonant frequencies of the cavity. The relative magnitudes of the $\hat{y}$-directed electric fields within the central portion of the cavity were measured as insertion loss, $S_{21}$, using a small coaxial probe (length = 0.95 cm, diameter = 0.30 cm) inserted into holes in the side of the cavity opposite from the excitation probe at $y = b$.

Several resonant modes were measured in the cavity. Measurements and simulations for the first (symmetric) $LSE_{101}$ mode are presented here. Table I shows the predicted and measured values of resonant frequency for this mode. Additionally, a relative topographical representation of the electric field measurements and a corresponding topograph of the simulated electric field values are included as Fig. 3. The simulated electric field distribution is normalized to the maximum measured value of $S_{21}$ to allow direct comparison of the field contours.

A swept frequency measurement of the cavity's unloaded $Q$ was taken using the HP 8753A Network Analyzer, following the procedure outlined by Aitken [10]. Table I includes the results of the calculation and measurement of the cavity's unloaded $Q$.

## V. DISCUSSION

Comparison between measured and simulated resonant frequencies and field distributions shows good agreement. The slightly higher measured values of electric fields at the center of the cavity are not present in the simulated values, probably due to the effect of the coaxial feed that is not taken into account in the simulations. One interesting aspect of these measurements and simulations is that while the cavity of interest has, in theory, identical dimensions in the $\hat{x}$ and $\hat{z}$ directions, the field patterns within the cavity for the $LSE_{101}$ mode (both calculated and measured) are not identical in these two directions, as evidenced by the elliptical shape of the contours. The behavior of the calculations may be explained by the fact that use of the effective length in $z$ necessarily predicts slightly different variations in $x$ and $z$. The measurements, on the other hand, indicate variations in $x$ and $z$ because the cavity dimensions of $a$ and $d$ were not exactly equal. If a cavity with $a$ and $d$ strictly equal were constructed, simulations would still indicate the same variations as those shown in Fig. 3, while the measurements of such a cavity would show completely identical variations in $x$ and $z$.

Given the latitude of the approximations used in the calculation of unloaded quality factor, the difference between the simulated and measured values of unloaded $Q$ presented in Table I is not as large as one might reasonably expect. Aside from errors inherent in the simulation model, differences between measured and simulated $Q$ may be due in part to variations in the relative permittivity and loss tangent of the loading slabs. The unloaded $Q$ of the slab-loaded cavity is much lower than that expected for an empty cavity (typically $\approx$ 10 000) for two reasons. First, loading of a resonant cavity with dielectric material lowers its $Q$ [9]. Second, insertion of lossy loading slabs into an empty cavity results in increased dielectric losses, which also reduce the cavity's $Q$.

## VI. CONCLUSION

This investigation demonstrates that a closed-form theoretical analysis may be modified to extend to structures that would otherwise be inappropriate for such an analysis. The approximations made for the dielectric slab-loaded resonant cavity provide quite accurate predictions of resonant frequency and electric field distributions, and good estimates of unloaded cavity $Q$.

The field distributions of the lowest order mode within the central portion of the slab-loaded cavity have a much smaller variation than an analogous mode in an empty rectangular cavity as shown in Fig. 2. Additionally, the presence of the high-permittivity loading slabs greatly reduces the bandwidth between resonant frequencies. These two observations translate to an exposure chamber that can deliver relatively uniform power to small samples in single-mode operation, and be swept over a relatively small band of frequencies to enlarge the available exposure volume.

While multimode cavities have been shown to have uniform power distributions when empty, the introduction of any sample material changes the boundary conditions within the cavity and consequently, the field distributions of each of the resonant modes. Calculating the effect of the sample on each particular mode to predict power deposition may prove cumbersome. However, with fewer and more spatially efficient modes present in the slab-loaded cavity, such calculations will be straightforward and accurate. Work is currently underway to predict power deposition achieved in the central regions of slab-loaded cavities completely and partially filled with sample material.

## REFERENCES

[1] M. F. Iskander, R. L. Smith, A. O. M. Andrade, H. Kimrey, and L. M. Walsh, "FDTD simulation of microwave sintering of ceramics in multimode cavities," *IEEE Trans. Microwave Theory Tech.*, vol. 42, pp. 793–800, May 1994.

[2] R. J. Lauf, D. W. Bible, A. C. Johnson, and C. A. Everleigh, "2 to 18 GHz broadbend microwave heating systems," *Microwave J.*, vol. 36, pp. 24–34, Nov. 1993.
[3] D. Rotkovska, A. Bartonickova, and J. Kautska, "Effects of microwaves on membranes of hematopoietic cells in their structural and functional organization," *Bioelectromagnetics,* vol. 14, pp. 79–85, 1993.
[4] E. R. Adair, B. W. Adams, and S. K. Hartman, "Physiological interaction processes and radio-frequency energy absorption," *Bioelectromagnetics,* vol. 13, pp. 497–512, 1992.
[5] R. E. Collin, *Field Theory of Guided Waves.* New York: McGraw-Hill, 1960, ch. 6.
[6] F. E. Gardiol, "Higher-order modes in dielectrically loaded rectangular waveguides," *IEEE Trans. Microwave Theory Tech.,* vol. MTT-16, pp. 919–924, Nov. 1968.
[7] C. A. Barlow, Jr. and E. Jones, "A method for the solution of roots of a nonlinear equation and for solution of the general eigenvalue problem," *J. ACM,* vol. 13, pp. 135–142, Jan. 1966.
[8] C. G. Montgomery, R. H. Dicke, and E. M. Purcell, Eds, *Principles of Microwave Circuits,* vol. 8, Radiation Laboratory Series. New York: McGraw-Hill, 1948.
[9] S. Ramo, J. R. Whinnery, and T. V. Duzer, *Fields and Waves in Communication Electronics.* New York: Wiley, 1984, ch. 10.
[10] J. Aitken, "Swept-frequency microwave $Q$-factor measurement," *Proc. IEE,* vol. 123, pp. 855–862, Sept. 1976.

# Variational Solution of Microwave Circuits and Structures

S. Tsitsos, N. Karamitsos, B. M. Dillon, and A. A. P. Gibson

***Abstract*— A unified variational formulation for microwave planar transmission lines and lumped-element impedances is developed and applied to an isolated stripline power splitter. Scattering parameters are calculated via the transfinite-element method and the numerical results are corroborated by three-port experimental measurements. The microwave impedance of a thin-film isolation resistor is separately measured and included in the model.**

## I. Introduction

Stripline power splitters with the appropriate power split ratio are cascaded together to produce the desired operative aperture field distribution in the corporate feeds of radar antenna systems [1]. Any distortion of the aperture excitation is minimized by using isolation load resistors suspended between coupled striplines to absorb reflected power [1]–[3]. This is one example of how highly irregular electromagnetic structures are often combined with lumped element components. Other examples range from varactor-tuned oscillators to high-directivity, capacitor-loaded directional couplers.

A new method that uses the variational solution of electrical circuits and fields is presented to cater for this class of problem. The transfinite-element method of Csendes and Lee [4] is extended to include lumped-element impedances and applied to an isolated stripline power splitter. Measured impedance data for a thin-film resistor is included in the model. Three-port scattering parameters and field plots are presented for an equal split junction. Experimental measurements are superimposed and compare well with the calculations. The amplitude of the $TE_{10}$ higher-order mode at the port reference planes has also been calculated.

Manuscript received December 8, 1994; revised November 27, 1995.

The authors are with Department of Electrical Engineering and Electronics, UMIST, Manchester, M60 1QD, U.K.

Publisher Item Identifier S 0018-9480(96)01550-5.

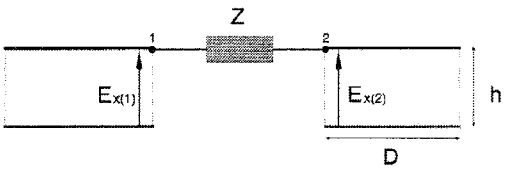


Fig. 1. Schematic of two planar waveguides with top and bottom electric walls and magnetic sidewalls connected via a lumped element impedance $Z$.

## II. Variational Formulation

Variational principles for electromagnetic resonators and waveguides were first introduced by Berk [5]. These expressions are often used with finite-element methods to predict modal hierarchy and scattering parameters in waveguides and junctions [4], [6]. Stationary energy methods can also be applied to electrical lumped-element networks [7]. Recently, a formal procedure describing the variational solution of linear and nonlinear circuits has been enunciated [8]. These methods are extended here to include interconnection with distributed planar transmission lines. The geometry in Fig. 1 depicts two planar waveguides connected via a lumped-element impedance Z. The power dissipated in this impedance is a function of the nodal terminal voltages $hE_{x(1)}$ and $hE_{x(2)}$ and is written as

$$P(E_x) = \frac{|E_{x(1)} - E_{x(2)}|^2 h^2}{Z}. \tag{1}$$

Following Csendes and Lee the variational functional for the planar waveguide sections is given by

$$F(E_x) = \frac{h}{j\omega\mu}\left[\int\int_A (|\nabla E_x|^2 - \omega^2\epsilon\mu|E_x|^2)\,dA - \sum_{i=1}^{P}\oint_{\Gamma_i} E_x^*\frac{\partial E_x}{\partial n}\,d\Gamma\right]. \tag{2}$$

The area integral refers to the layout of a planar geometry and represents the stored electromagnetic energy. The line integral represents the power flow onto each port $p$. The permittivity, permeability, and angular signal frequency are denoted $\epsilon$, $\mu$, and $\omega$, respectively. For planar waveguides interconnected or terminated by Q-lumped element impedances, (1) and (2) are combined as [9]

$$F(E_x) = \sum_{q=1}^{Q}\frac{|E_{x(i)} - E_{x(k)}|^2 h^2}{Z_q} + \frac{h}{j\omega\mu}\left[\int\int_A (|\nabla E_x|^2 - \omega^2\epsilon\mu|E_x|^2)\,dA - \sum_{i=1}^{P}\oint_{\Gamma_i} E_x^*\frac{\partial E_x}{\partial n}\,d\Gamma\right] \tag{3}$$

where each impedance $Z_q$ is connected between nodes $i$ and $k$ of a finite-element mesh.

## III. Stripline Formulation

The transfinite-element method described by [4] uses a planar waveguide transformation to model microstrip-like transmission lines. An efficient two-dimensional analysis of three-dimensional microstrip discontinuities and junctions then follows. Triplate stripline can be transformed into two parallel plate waveguides one on top of the other. Each waveguide has top and bottom electric walls and magnetic